Supporting Information

Spin Transitions in $[Fe(pybox)_2]^{2+}$ Series Complexes Modulated by Ligand Structures, Counter Anions, and Solvents

Yuan-Yuan Zhu,[a] Hong-Qing Li,[a] Zhong-Yu Ding,[a] Xiao-Jin Lü,[b] Liang Zhao,[b] Yin-Shan Meng,[c] Tao Liu,*[b] and Song Gao[c]*

[a]School of Chemistry and Chemical Engineering, Hefei University of Technology and Anhui Key Laboratory of Advanced Functional Materials and Devices, Hefei 230009, China, E-mail: yyzhu@hfut.edu.cn

[b]State Key Laboratory of Fine Chemicals, Dalian University of Technology, 2 Linggong Road, Dalian 116024, China, E-mail: liutao@dlut.edu.cn

[c]Beijing National Laboratory for Molecular Sciences, State Key Laboratory of Rare Earth Materials Chemistry and Applications, College of Chemistry and Molecular Engineering, Peking University, Beijing 100871, China

List of Supporting Information

SI1 Synthesis details

Synthesis of the pybox ligands

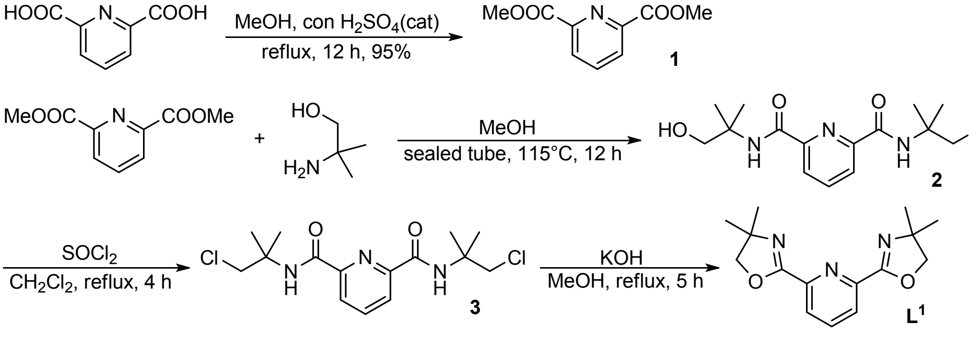

Scheme S1

Compound 1.[1] To pyridine-2,6-dicarboxylic acid (3.34 g, 20 mmol) in methanol (20 mL) was added con H_2SO_4 (0.5 mL) dropwise and slowly, the solution was stirred at reflux for 12 hours and the insoluble powder was gradually dissolved. After cooled to room temperature, the solution was concentrated under reduced pressure and the crude product was dissolved in EtOAc (30 mL) and washed with deionized H_2O (10 mL × 2), saturated aqueous $NaHCO_3$ (10 mL), and brine (10 mL) and dried over sodium sulfate. The solvent was removed and give **1** as a white solid (3.70 g, 95%) without further purification.

Compound 2.[2] A mixture of **1** (1.95 g, 10 mmol) and 2-amino-2-methylpropan-1-ol (1.78 g, 20 mmol) was stirred in methanol (10 mL) at 115 ºC in sealed tube for 12 h. After cooled to room temperature, the solution was concentrated under reduced pressure. The resulting residue was subjected to column chromatography (SiO_2, dichloromethane/methanol, 20:1) to afford **2** as a white solid (2.94 g, 95%). ^1H NMR (600 MHz, $CDCl_3$): δ 8.32 (d, J = 7.8 Hz, 2 H), 8.04 (t, J = 7.8 Hz, 1 H), 8.02 (br, 2 H), 3.98 (br, 2 H), 3.72 (d, J = 5.4 Hz, 4 H), 1.47 (s, 12 H).

Compound 3.[3] A solution of **2** (2.94 g, 9.5 mmol) in dichloromethane (10 mL) was cooled in an ice bath, then $SOCl_2$ (10 mL) was added dropwise, and then the solution was stirred at reflux for 2 h. After cooled to room temperature, the solution was concentrated under reduced pressure and the resulting residue was triturated with dichloromethane (20 mL). The solution was washed with deionized H_2O (10 mL × 2), saturated aqueous $NaHCO_3$ (10 mL), and brine (10 mL) and dried over sodium sulfate. After the solvent was removed, the crude product was subjected to column chromatography (SiO_2, dichloromethane/EtOAc, 20:1) to give **3** as a white solid (2.89 g, 88%). ^1H NMR (400 MHz, $CDCl_3$): δ 8.27 (d, J = 7.8 Hz, 2 H), 8.00 (t, J = 7.8 Hz, 1 H), 7.90 (br, 2 H), 3.85 (s, 4 H), 1.55 (s, 12 H).

Compound L^1.[3] To a solution of **3** (1.73 g, 5 mmol) in methanol (25 mL) was added KOH (0.7 g, 12.5 mmol), the solution was stirred at reflux for 4 h and white precipitation was generated during the reaction. The solution was concentrated under reduced pressure. The resulting residue was triturated with dichloromethane (30 mL) and the solution washed with water (15 mL × 3) and brine (15 mL) and dried over sodium sulfate. Compound **L** was obtained as white solid under vacuum drying (1.30 g, 95%).

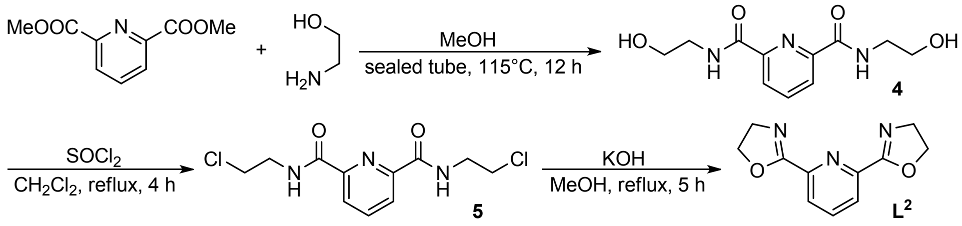

Scheme S2

Compound 4.[2] A mixture of **1** (1.95 g, 10 mmol) and 2-aminoethanol (1.34 g, 22 mmol) was stirred in methanol (10 mL) at 115 ºC in sealed tube for 12 h. The solution was concentrated in vacuo and the residue was purified by column chromatography (SiO_2, CH_2Cl_2/MeOH 20:1) to give **4** as white solid product (2.41 g, 95%). ^{1}H NMR (400 MHz, DMSO-d_6): δ 9.36 (t, J = 6.0 Hz, 2 H), 8.20-8.12 (m, 3 H), 4.84 (t, J = 5.6 Hz, 2 H), 3.57 (q, J = 6.0 Hz, 4 H), 3.43 (q, J = 6.0 Hz, 4 H).

Compound 5.[2] A solution of **4** (2.41 g, 9.5 mmol) in dichloromethane (10 mL) was cooled in an ice bath, then $SOCl_2$ (10 mL) was added dropwise, and then the solution was stirred at reflux for 2 h. The solution was concentrated under reduced pressure and the resulting residue was triturated with dichloromethane (20 mL). The solution was washed with deionized H_2O (10 mL × 2), saturated aqueous $NaHCO_3$ (10 mL), and brine (10 mL) and dried over sodium sulfate. After the solvent was removed, the crude product was subjected to column chromatography (SiO_2, petroleum ether (PE)/AcOEt 2:1 to 1:1) to give **3** as a white solid (2.34 g, 85%). ^{1}H NMR (400 MHz, $CDCl_3$): δ 8.36 (d, J = 8.0 Hz, 2 H), 8.27 (br, 2 H), 8.05 (t, J = 7.6 Hz, 1 H), 3.87-3.82 (m, 4 H), 3.74 (t, J = 5.6 Hz, 4 H).

Compound L^2.[3] To a solution of **3** (1.45 g, 5 mmol) in methanol (25 mL) was added KOH (0.7 g, 12.5 mmol), the solution was stirred under reflux for 4 hours and white precipitation was generated during the reaction. The solution was concentrated under reduced pressure. The resulting residue was triturated with dichloromethane (30 mL) and the solution washed with water (15 mL) and brine (15 mL) and dried over sodium sulfate. Compound **L^1** was obtained as white solid under vacuum drying (1.03 g, 95%). ^{1}H NMR (400 MHz, $CDCl_3$): δ 8.15 (d, J = 8.0 Hz, 2 H), 7.86 (t, J = 8.0 Hz, 1 H), 4.52 (t, J = 10.0 Hz, 4 H), 4.10 (t, J = 10.0 Hz, 4 H).

References

1. Y.-Y. Zhu, C. Cui, N. Li, B.-W. Wang, Z.-M. Wang, S. Gao, *Eur. J. Inorg. Chem.* **2013**, *17*, 3101.
2. B. P. Bandgar, S. S. Pandit, *Tetrahedron Lett.* **2003**, *44*, 2331.
3. F. Ito, T. Nakamura, S. Yorita, H. Danjo, K. Yamaguchi, *Tetrahedron Lett.* **2009**, ***50***, 6252.

^{1}H NMR spectra

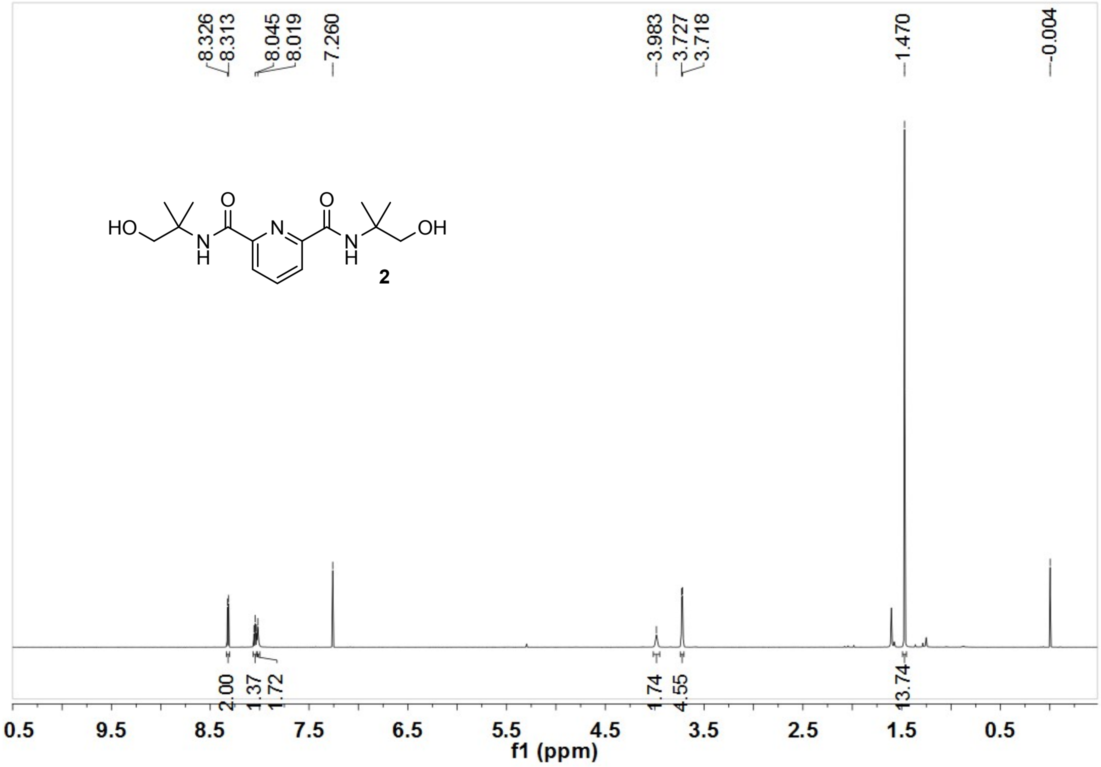

Figure S1. ^{1}H NMR spectrum of compound **2** (600 MHz) in $CDCl_3$ (10 mM).

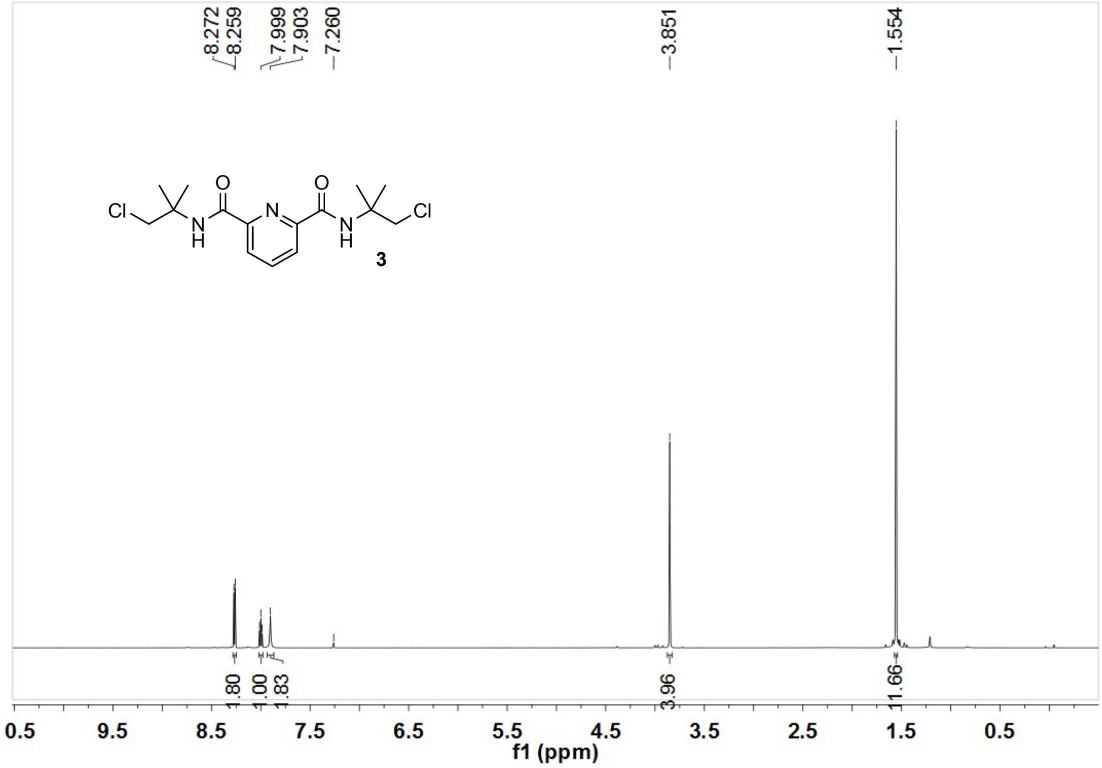

Figure S2. ^{1}H NMR spectrum of compound **3** (600 MHz) in $CDCl_3$ (10 mM).

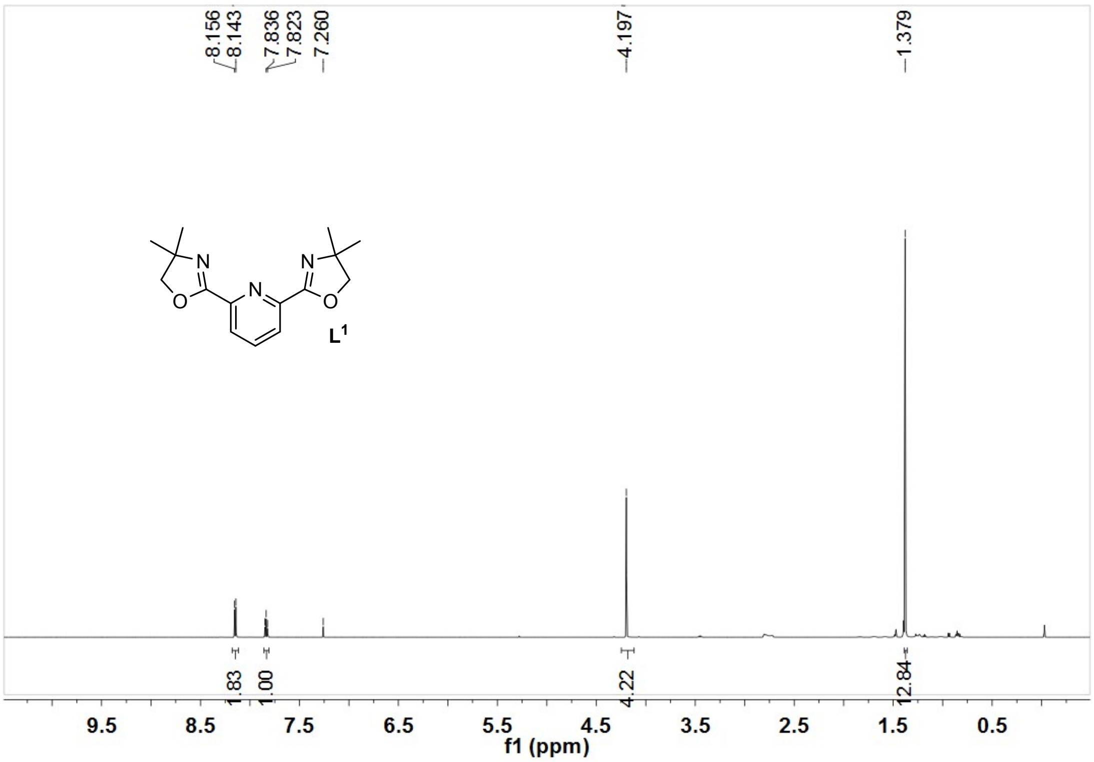

Figure S3. ^{1}H NMR spectrum of compound **L^{1}** (600 MHz) in $CDCl_3$ (10 mM).

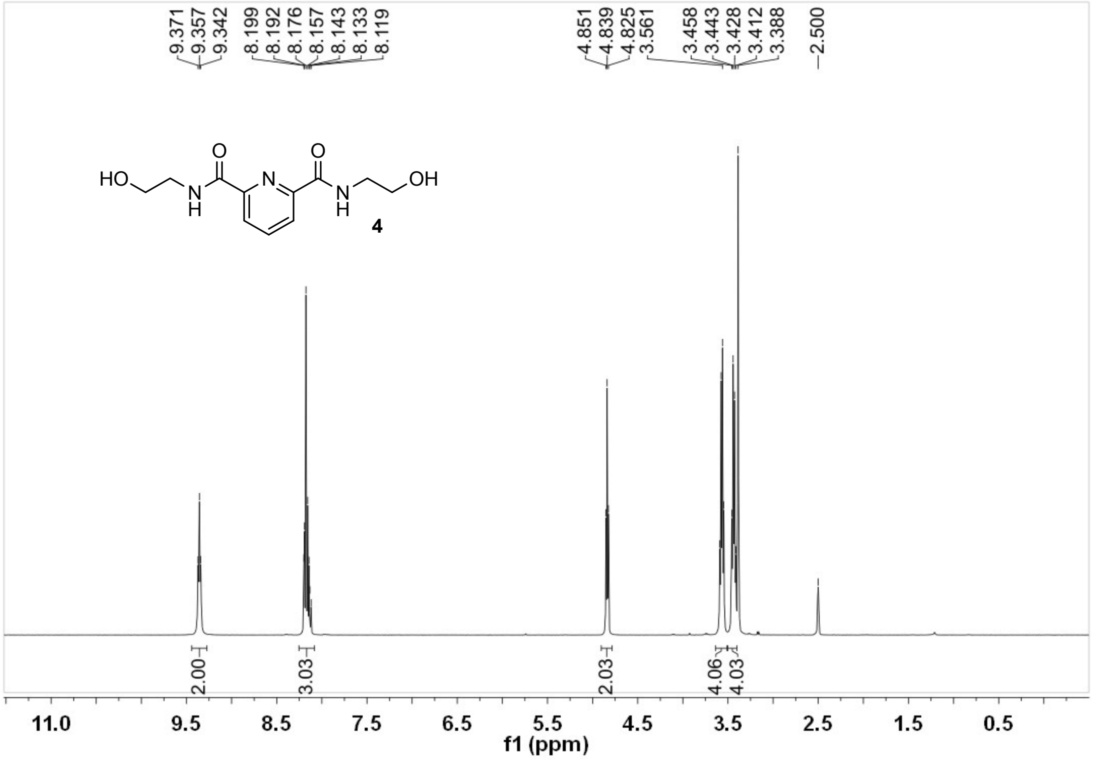

Figure S4. ^{1}H NMR spectrum of compound **4** (400 MHz) in DMSO-d_6 (10 mM).

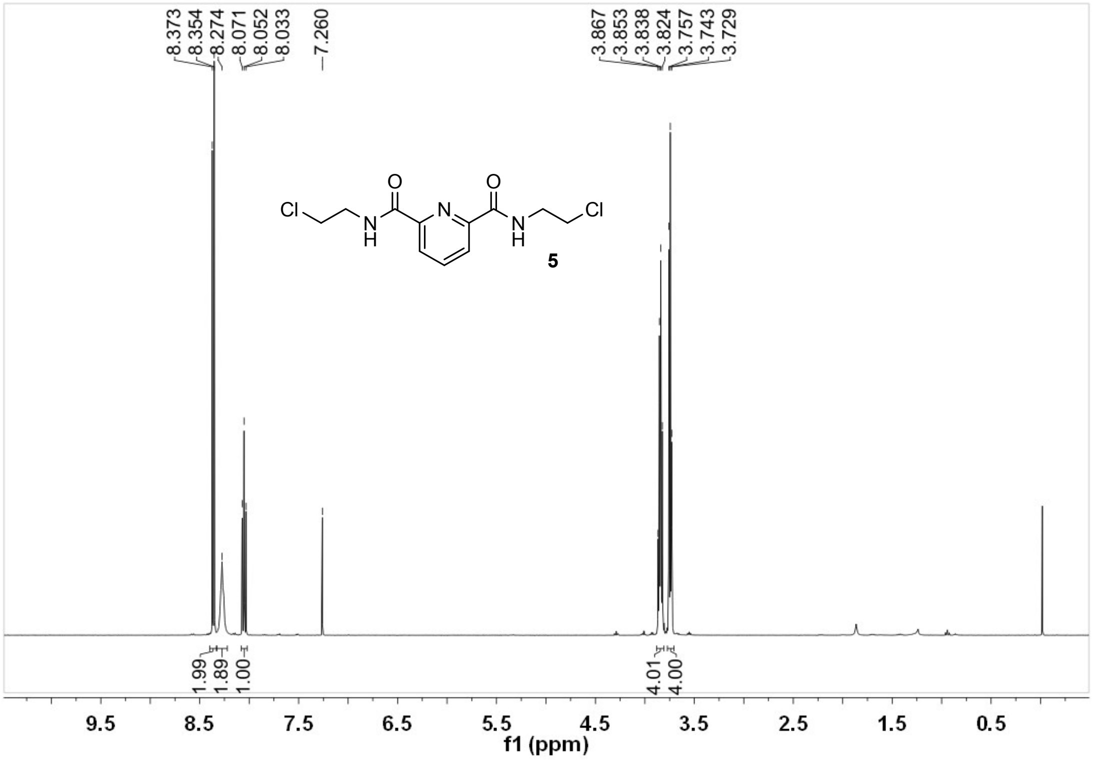

Figure S5. ^{1}H NMR spectrum of compound **5** (400 MHz) in $CDCl_3$ (10 mM).

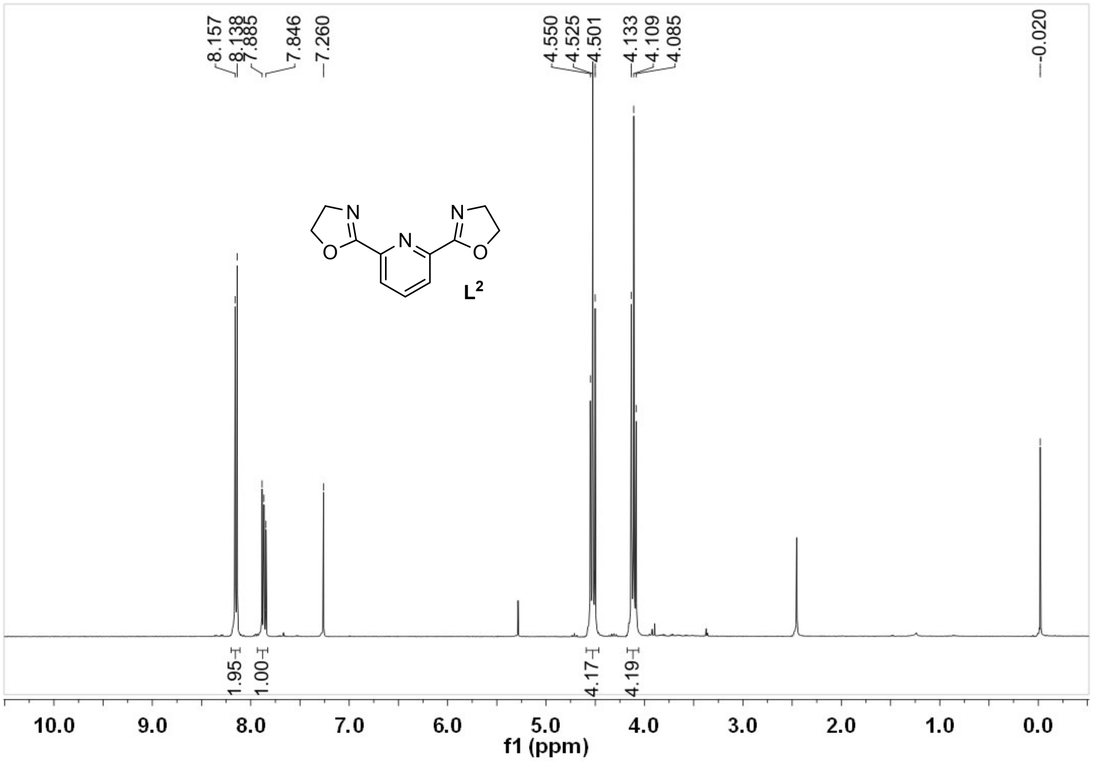

Figure S6. ^{1}H NMR spectrum of compound **L^2** (400 MHz) in $CDCl_3$ (10 mM).

SI2 Structure details

Table S1. Crystal data, data collection, solution, and refinement information of iron(II) compounds in this work.

	1(BF_4)	**1(BF_4)**	**1(BF_4)·MeCN**	**1(PF_6)·MeCN·Et_2O**	**1(BPh_4)·MeCN**	**1(BPh_4)·MeCN**	**2(ClO_4)**
Formula	$C_{30}H_{38}B_2F_8FeN_6O_4$	$C_{60}H_{76}B_4F_{16}Fe_2N_{12}O_8$	$C_{32}H_{41}B_2N_7O_4F_8Fe$	$C_{66}H_{89}N_{13}O_9F_{24}P_4Fe_2$	$C_{78}H_{78}B_2FeN_6O_4$	$C_{78}H_{78}B_2FeN_6O_4$	$C_{22}H_{22}N_6O_{12}Cl_2Fe$
formula weight	776.13	1552.26	817.19	1900.08	1240.93	1240.93	689.20
crystal system	orthorhombic	monoclinic	orthorhombic	triclinic	monoclinic	monoclinic	monoclinic
space group	*P*bca	$P2_1/c$	*P*bca	$P\bar{1}$	*P*2/c	*P*2/c	$P2_1/n$
a, Å	13.6828(4)	13.6930(5)	16.918(3)	14.1084(19)	23.3002(4)	23.401(2)	15.386(3)
b, Å	19.9361(6)	19.5154(7)	18.982(4)	16.260(2)	13.24618(16)	13.5170(13)	10.700(2)
c, Å	25.5286(8)	24.9934(11)	23.007(5)	19.256(4)	24.3060(4)	24.582(2)	16.934(3)
α, deg	90	90	90	101.206(2)	90	90	90
β, deg	90	92.184(4)	90	91.086(2)	114.454(2)	113.656(1)	103.31(3)
γ, deg	90	90	90	101.768(2)	90	90	90
V, Å^3	6963.7(4)	6674.0(5)	7388(3)	4234.1(12)	6828.8(2)	7122.2(12)	2713.2(10)
Z	8	4	8	2	4	4	4
T, K	180(1)	120(2)	153(2)	296(2)	180(2)	296(2)	173(2)
F(000)	3200	3200	3376	1952	2624	2624	1408
D_C, g cm^{-3}	1.481	1.545	1.469	1.490	1.207	1.157	1.687
μ, mm^{-1}	0.521	4.440	0.495	0.530	2.191	0.264	0.829
λ, Å	0.71073	1.54178	0.71073	0.71073	1.54184	0.71073	0.71073
crystal size, mm^3	0.45 × 0.42 × 0.33	0.38 × 0.35 × 0.33	0.53 × 0.45 × 0.37	0.45 × 0.40 × 0.31	0.35 × 0.31 × 0.25	0.38 × 0.36 × 0.26	0.32 × 0.22 × 0.18
T_{min} and T_{max}	0.78931, 1.00000	0.36980, 1.0000	0.8961, 1.0000	0.6438, 0.7455	0.7754, 1.0000	0.6807, 0.7455	0.5755, 1.0000
θ_{min}, θ_{max}, deg	3.5000, 28.3000	2.8490, 74.1620	2.3949, 29.1051	2.29, 25.71	3.3070, 73.6520	1.9, 52.044	1.2356, 27.4849
no. total reflns.	16562	16106	26358	32821	27190	53558	17804
no. uniq. reflns, R_{int}	9640, 0.0470	13091, 0.0753	9874, 0.0423	16754, 0.0367	13256, 0.0246	13913, 0.0465	6190, 0.0597
no. obs. [$I \geq 2\sigma(I)$]	6564	10986	9537	16754	10991	8448	6190
no. params	496	955	496	1082	828	828	425
*R*1 [$I \geq 2\sigma(I)$]	0.0531	0.1187	0.0663	0.0711	0.0379	0.0480	0.0585
*wR*2 (all data)	0.1486	0.3517	0.1366	0.2311	0.1002	0.1274	0.1227
S	1.028	1.158	1.264	1.022	1.055	1.009	1.115
$\Delta\rho^a$, *e* / Å^3	0.885, –0.923	3.074, –1.096	0.559, –0.463	0.93, –0.61	0.388, –0.350	0.207, –0.278	0.40, –0.41
max. and mean Δ / σ^b	0.001, 0.000	0.000, 0.000	0.001, 0.000	0.001, 0.000	0.002, 0.000	0.001, 0.000	0.001, 0.000
CCDC	1468980	1507077	1468981	1468982	1468983	1468984	1468985

Continued Table

	2(BF$_4$)	**2(PF$_6$)·MeCN**	**2(PF$_6$)·MeCN**	**2(BPh$_4$)**	**2(BPh$_4$)**	**2(BPh$_4$)**
Formula	$C_{22}H_{22}B_2N_6O_4F_8Fe$	$C_{24}H_{25}F_{12}FeN_7O_4P_2$	$C_{24}H_{25}F_{12}FeN_7O_4P_2$	$C_{35}H_{31}N_{2.5}O_2BFe_{0.5}$	$C_{35}H_{31}N_{2.5}O_2BFe_{0.5}$	$C_{35}H_{31}N_{2.5}O_2BFe_{0.5}$
formula weight	663.92	821.30	821.30	564.36	564.36	564.36
crystal system	monoclinic	monoclinic	Monoclinic	tetragonal	tetragonal	tetragonal
space group	$P2_1/n$	$P2_1/c$	$P2_1/c$	$I4_1/a$	$I4_1/a$	$I4_1/a$
a, Å	15.5545(11)	15.352(3)	15.103(3)	17.4289(4)	17.51122(11)	17.6175(3)
b, Å	10.6057(8)	10.908(2)	11.142(2)	17.4289(4)	17.51122(11)	17.6175(3)
c, Å	17.0270(12)	20.708(4)	20.558(4)	37.4287(13)	37.5872(4)	37.7194(10)
α, deg	90	90	90	90	90	90
β, deg	103.9860(10)	102.05(3)	102.330(2)	90	90	90
γ, deg	90	90	90	90	90	90
V, Å^3	2725.6(3)	3391.2(12)	3379.7(13)	11369.6(6)	11525.85(19)	11707.2(5)
Z	4	4	4	16	16	16
T, K	296(2)	153(2)	296(2)	100	180	300
F(000)	1344	1656	1656	4680	4680	4680
D_c, g cm^{-3}	1.618	1.609	1.614	1.302	1.285	1.265
μ, mm^{-1}	0.650	0.647	0.649	0.322	2.533	0.313
λ, Å	0.71073	0.71073	0.71073	0.71073	1.54184	0.71073
crystal size, mm^3	0.45 × 0.33 × 0.27	0.40 × 0.34 × 0.21	0.30 × 0.26 × 0.18	0.35 × 0.31 × 0.26	0.44 × 0.38 × 0.27	0.35 × 0.31 × 0.26
T_{min} and T_{max}	0.6840, 0.7455	0.7083, 1.0000	0.6653, 0.7455	0.91147, 1.00000	0.8076, 1.0000	0.76591, 1.00000
θ_{min}, θ_{max}, deg	2.28, 26.57	2.0112, 28.8199	2.290, 24.391	5.924, 60.842	3.5110, 76.1490	3.4900, 24.1550
no. total reflns.	20162	21602	25228	35672	48043	86298
no. uniq. reflns, R_{int}	5321, 0.0224	6621, 0.0506	6604, 0.0292	7856, 0.0407	5656, 0.0486	5738, 0.0551
no. obs. [$I \geq 2\sigma(I)$]	4538	4146	4844	5696	5264	3953
no. params	388	452	452	376	376	376
$R1$ [$I \geq 2\sigma(I)$]	0.0552	0.0879	0.0585	0.0437	0.1410	0.0403
$wR2$ (all data)	0.1748	0.2731	0.1847	0.1124	0.3500	0.1202
S	1.044	1.022	1.042	1.027	1.097	1.036
$\Delta\rho^a$, e/ Å^3	1.40, −0.56	2.078, −0.742	0.827, −0.438	0.32, −0.50	0.641, −0.619	0.196, −0.250
max. and mean Δ/σ^b	0.000, 0.000	0.000, 0.000	0.000, 0.000	0.001, 0.000	0.000, 0.000	0.000, 0.000
CCDC	1468986	1468987	1468988	1468989	1468990	1468991

[a] Max and min residual density. [b] Max and mean shift/σ.

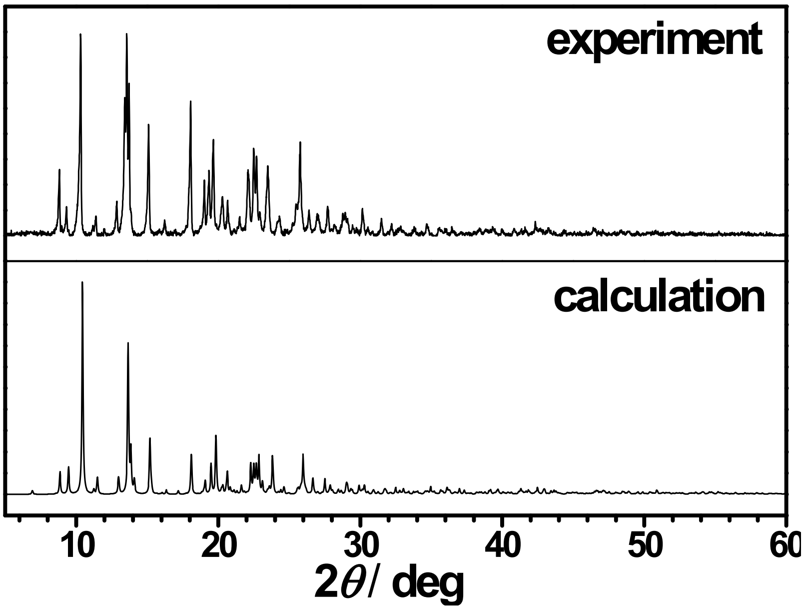

Figure S7. The powder XRD pattern of **1(BF$_4$)** and the simulated pattern from the single-crystal X-ray structure.

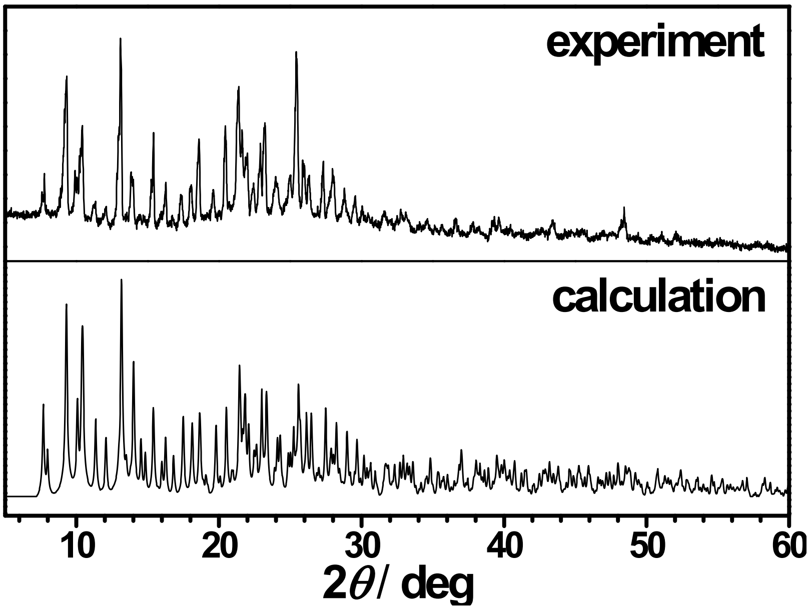

Figure S8. The powder XRD pattern of **1(BF$_4$)·MeCN** and the simulated pattern from the single-crystal X-ray structure.

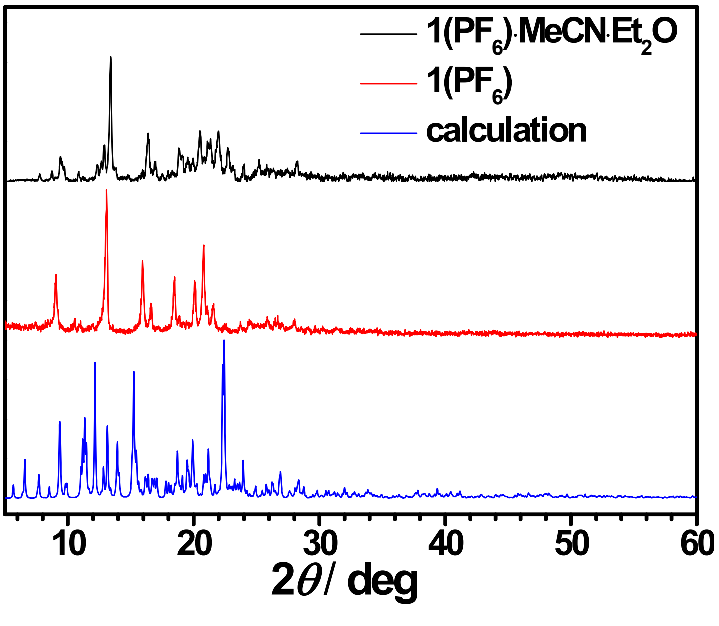

Figure S9. The powder XRD pattern of **1(PF$_6$)·MeCN·Et$_2$O**, desolvated sample **1(PF$_6$)** and the simulated pattern from the single-crystal X-ray structure, indicating the solvent is partial lost after grind of the crystals due to the loss of solvents.

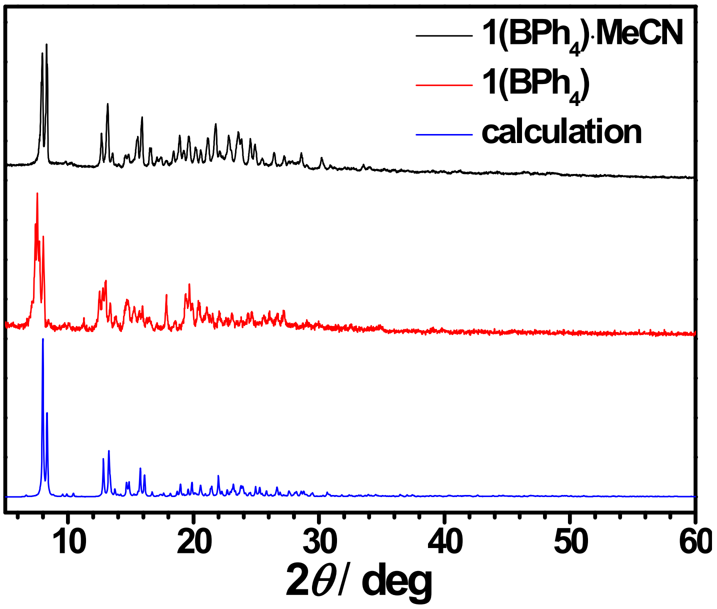

Figure S10. The powder XRD pattern of **1(BPh$_4$)·MeCN** and the simulated pattern from the single-crystal X-ray structure.

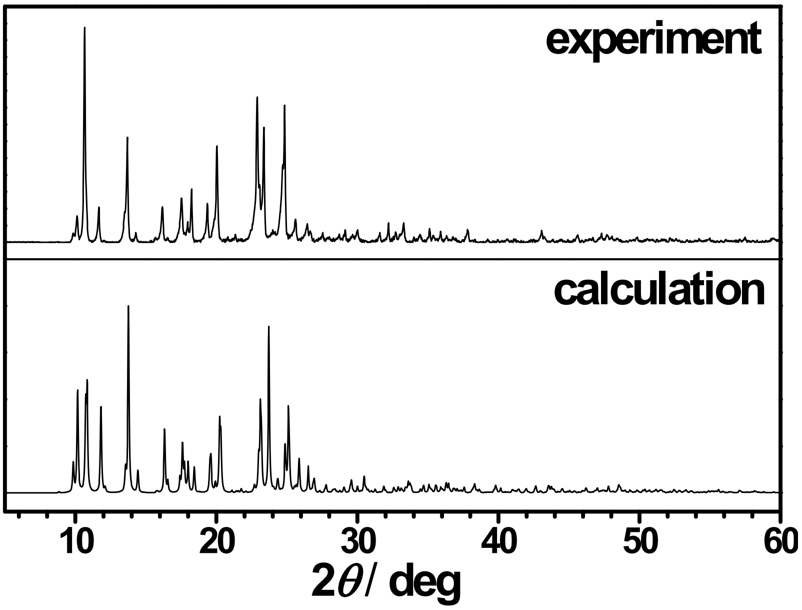

Figure S11. The powder XRD pattern of **2(ClO$_4$)** and the simulated pattern from the single-crystal X-ray structure.

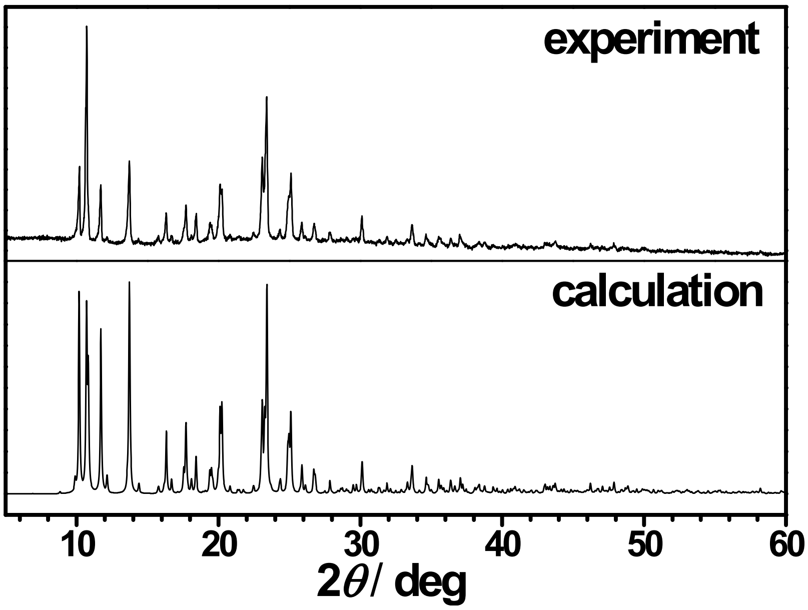

Figure S12. The powder XRD pattern of **2(BF$_4$)** and the simulated pattern from the single-crystal X-ray structure.

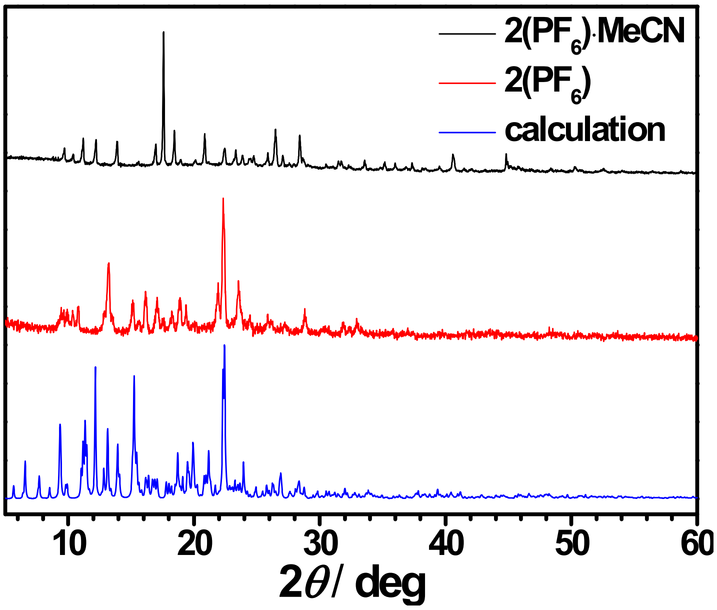

Figure S13. The powder XRD pattern of **2(PF$_6$)·MeCN** and the simulated pattern from the single-crystal X-ray structure, indicating the crystalline phase is changed after grind of the crystals due to the loss of solvents.

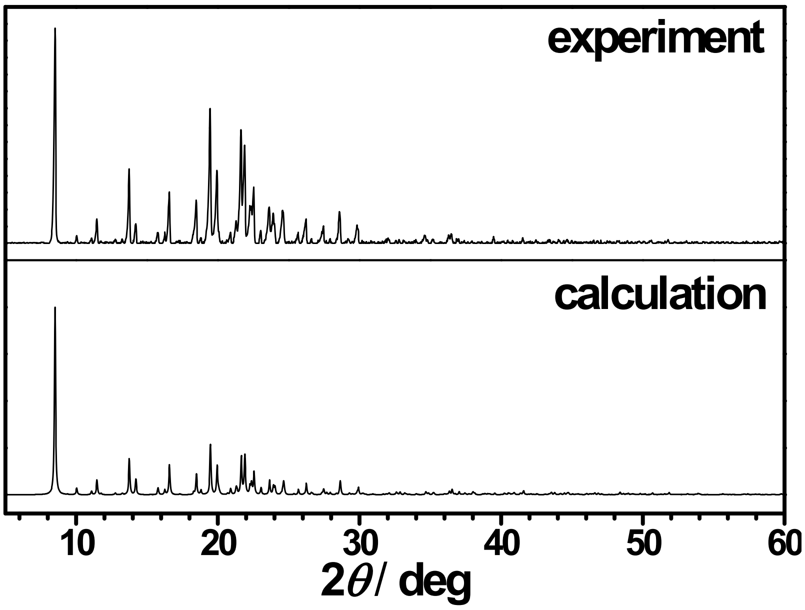

Figure S14. The powder XRD pattern of **2(BPh$_4$)** and the simulated pattern from the single-crystal X-ray structure.

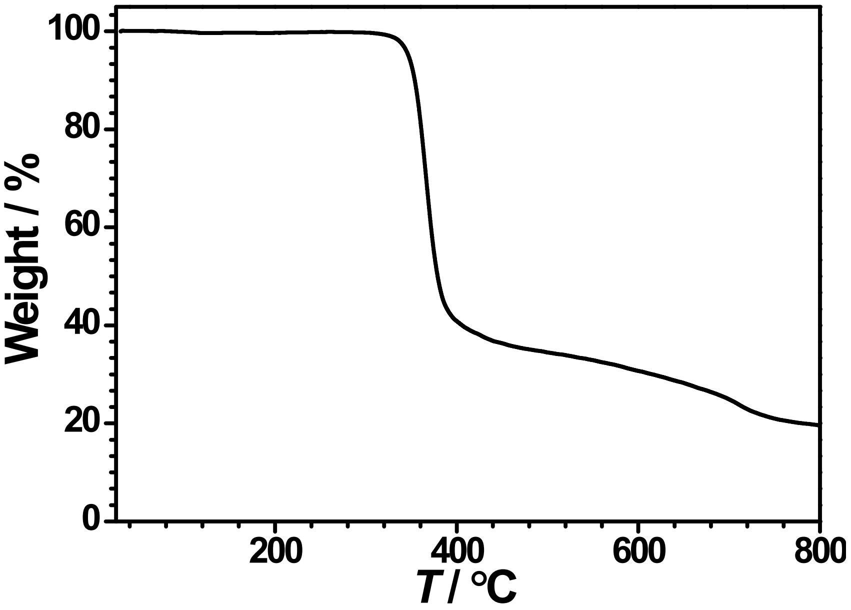

Figure S15. The TGA trace of **1(BF$_4$)**, indicating the decomposition of compound starts at 300 °C.

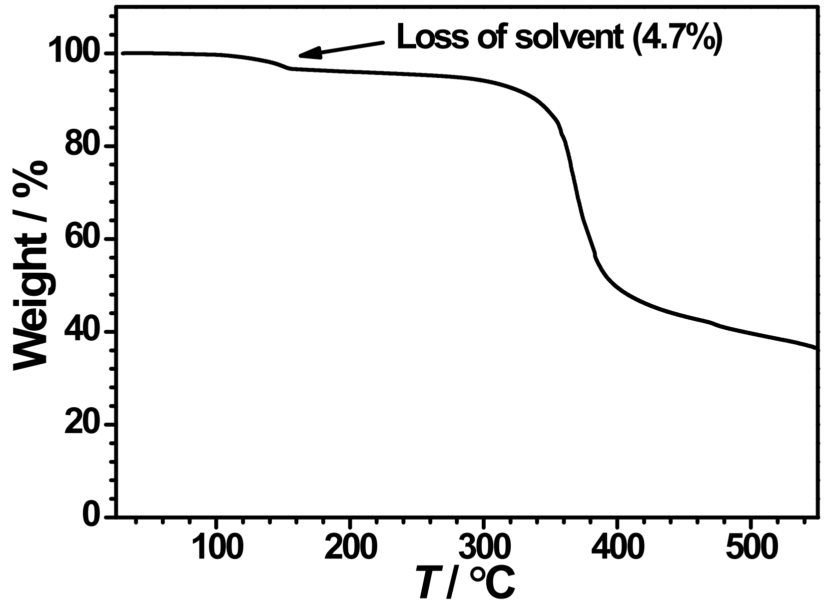

Figure S16. The TGA trace of **1(BF$_4$)·MeCN**, indicating the loss of acetonitrile completes below 200 °C.

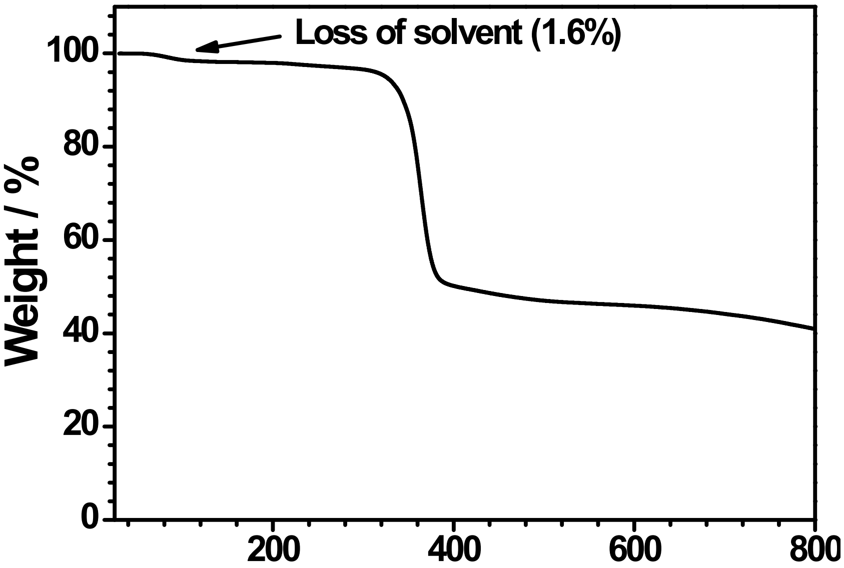

Figure S17. The TGA trace of **1(PF$_6$)·MeCN·Et$_2$O**, indicating the loss of acetonitrile completes below 200 °C.

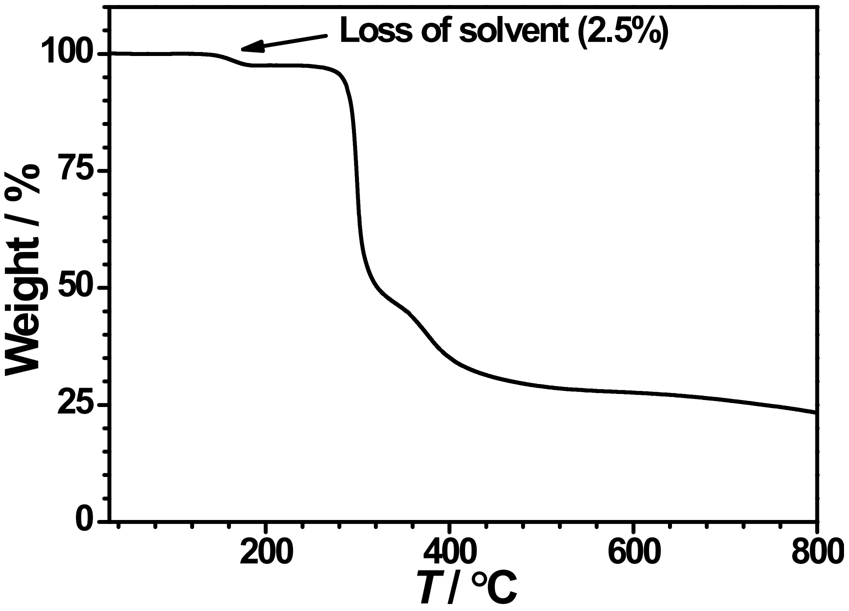

Figure S18. The TGA trace of **1(BPh$_4$)·MeCN**, indicating the loss of acetonitrile completes below 200 °C.

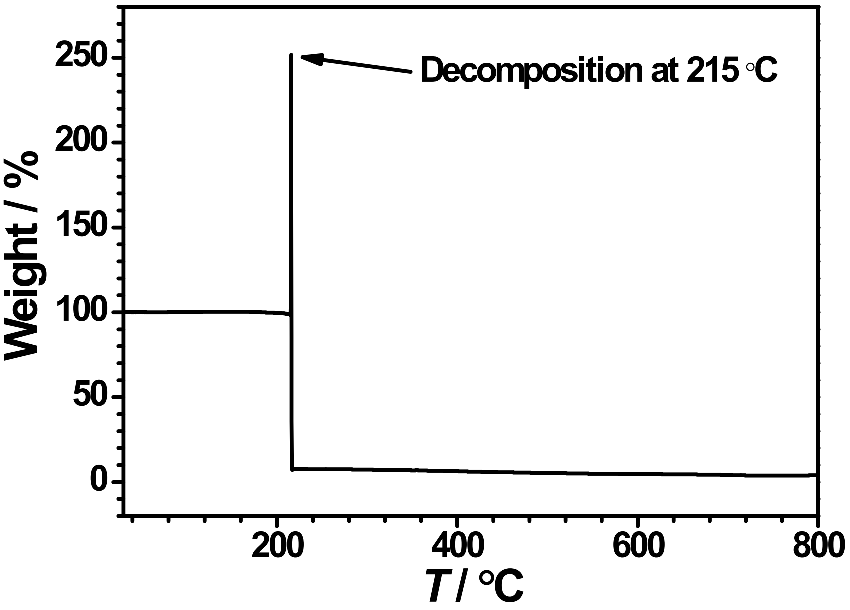

Figure S19. The TGA trace of **2(ClO$_4$)**, indicating the decomposition of compound starts at 215 °C.

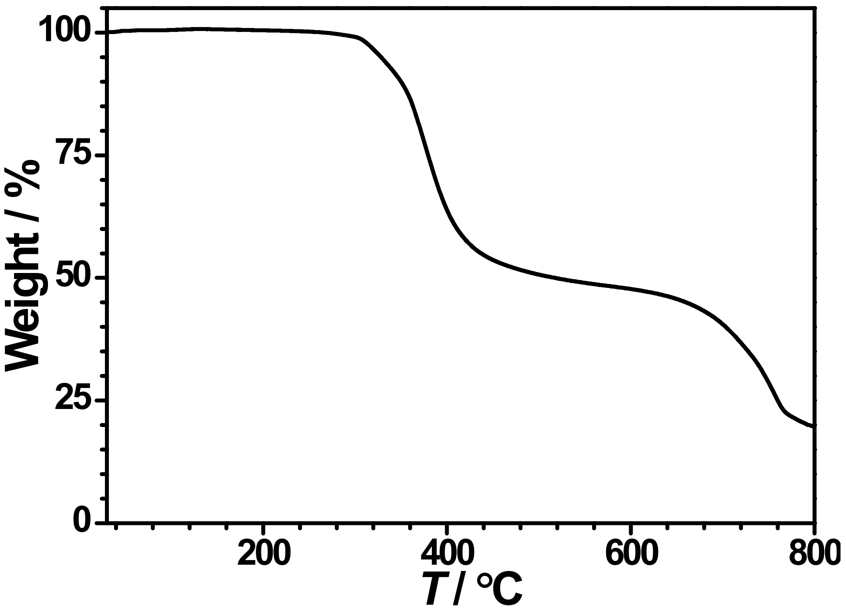

Figure S20. The TGA trace of **2(BF$_4$)**, indicating the decomposition of compound starts above 250 °C.

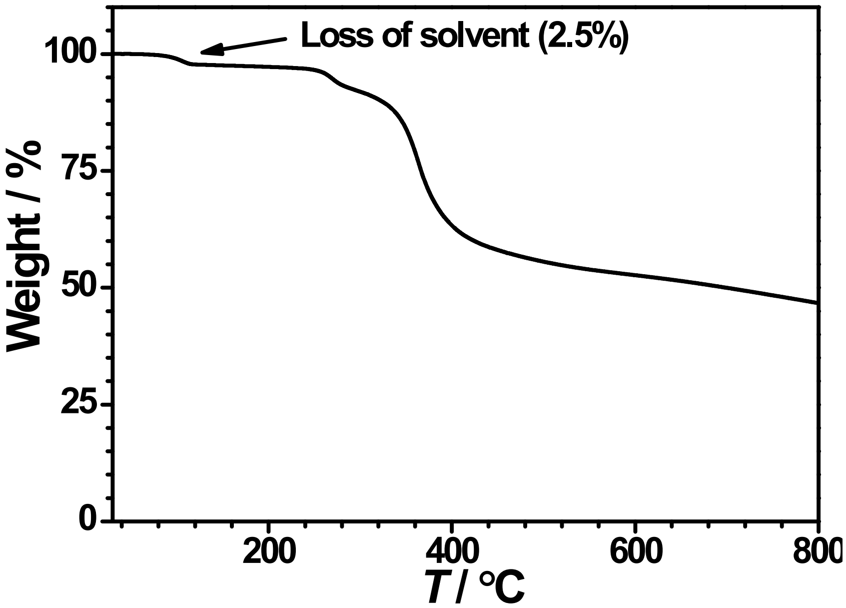

Figure S21. The TGA trace of **2(PF$_6$)·MeCN**, indicating the loss of acetonitrile completes below 200 °C.

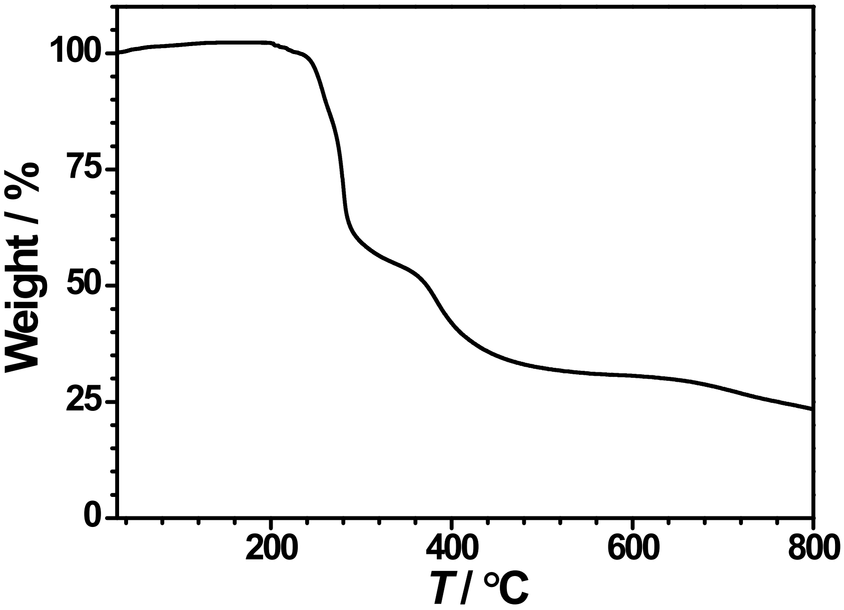

Figure S22. The TGA trace of **2(BF$_4$)**, indicating the decomposition of compound starts above 200 °C.

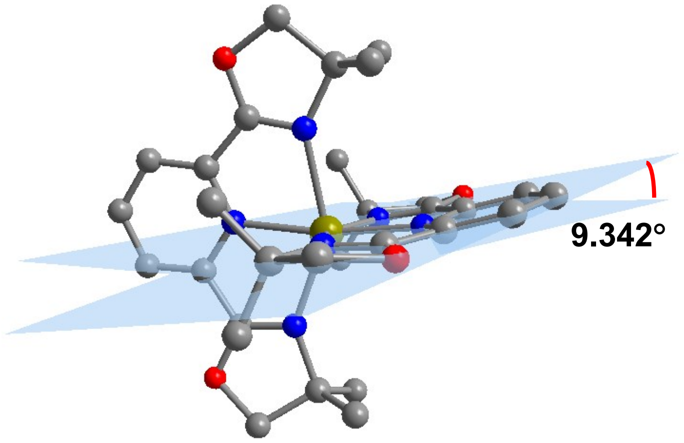

Figure S23. The bending angle between the pyridine ring plane and the pybox ligand plane (determined by three coordinated N atoms in one ligand) in **1(BF$_4$)·MeCN**.

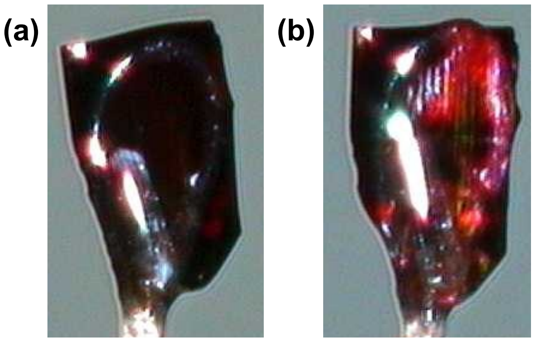

Figure S24. the photographs of the same single crystal of **1(BF$_4$)** at (a) 180 K (dark red) and (b) 100 K (red).

SI3 Properties measurements

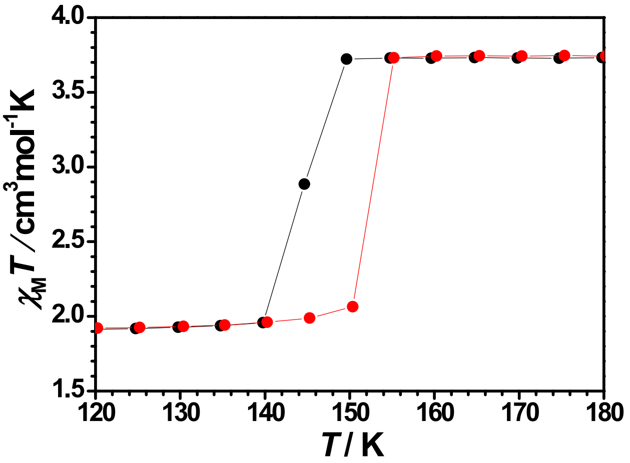

Figure S25. The thermal hysteresis loop of **1(BF$_4$)** with the width of about 5 K around 150 K.

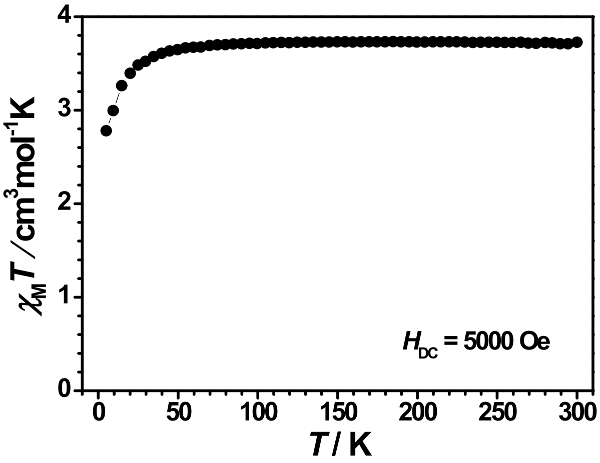

Figure S26. Plots of $\chi_M T$ *vs*. T for **1(BF$_4$)·MeCN**.

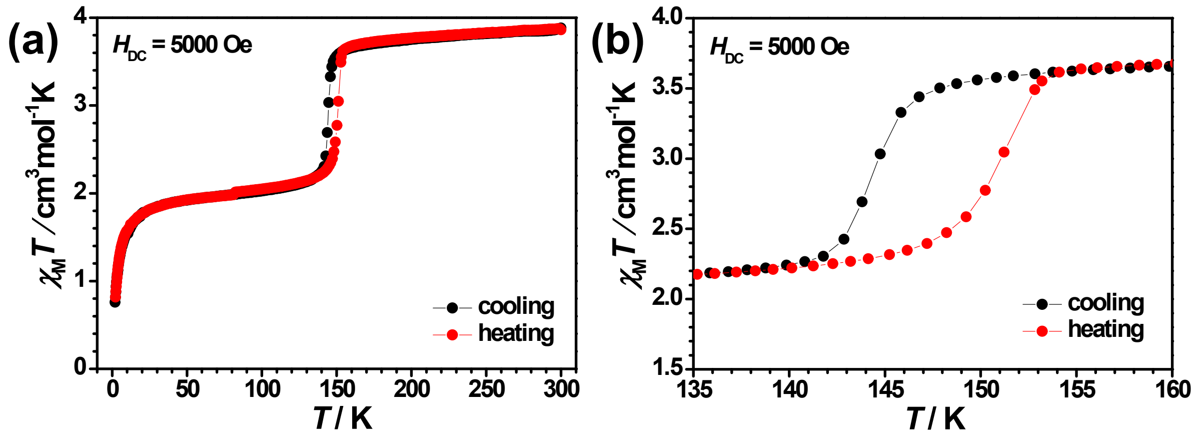

Figure S27. (a) Plots of $\chi_M T$ *vs*. T for **1(BF$_4$)'** (desolvated sample of **1(BF$_4$)·MeCN**) in the cooling and heating mode; (b) The thermal hysteresis loop of **1(BF$_4$)'** with the width of about 5 K around 150 K.

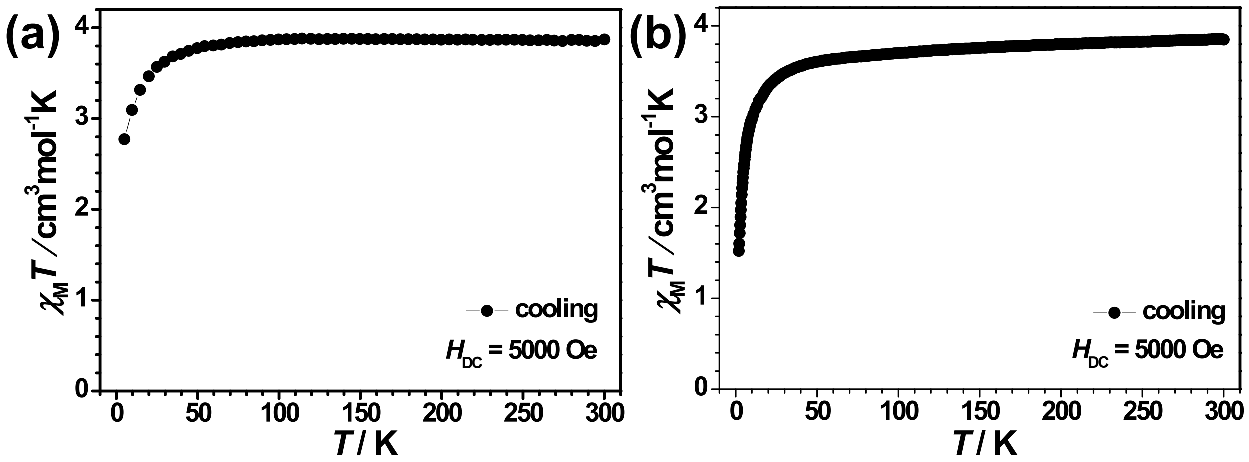

Figure S28. Plots of $\chi_M T$ *vs.* T for **1(PF$_6$)·MeCN·Et$_2$O** and desolvated sample **1(PF$_6$)**.

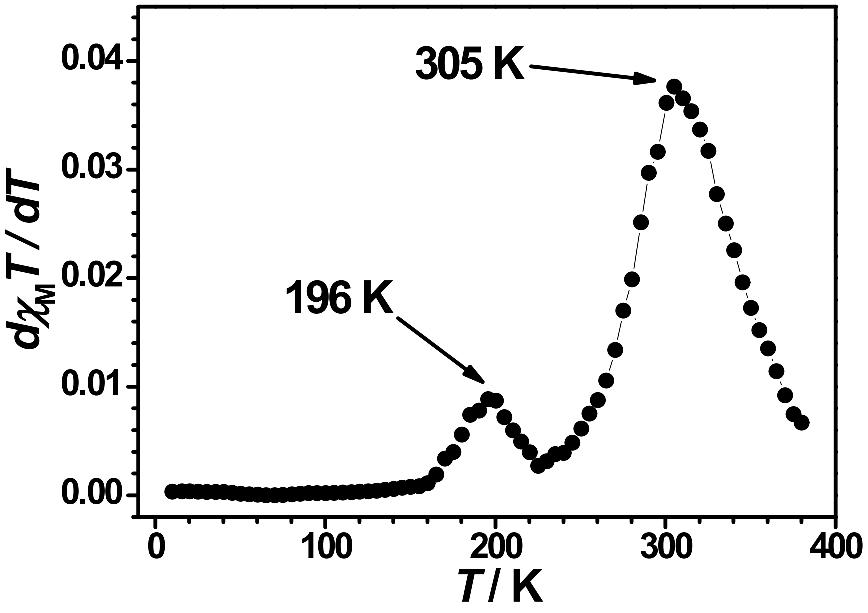

Figure S29. Plot of $d\chi_M T/dT$ *vs.* T for **2(PF$_6$)·MeCN**. The two peaks at 196 and 305 K reflect the two-step SCO process.

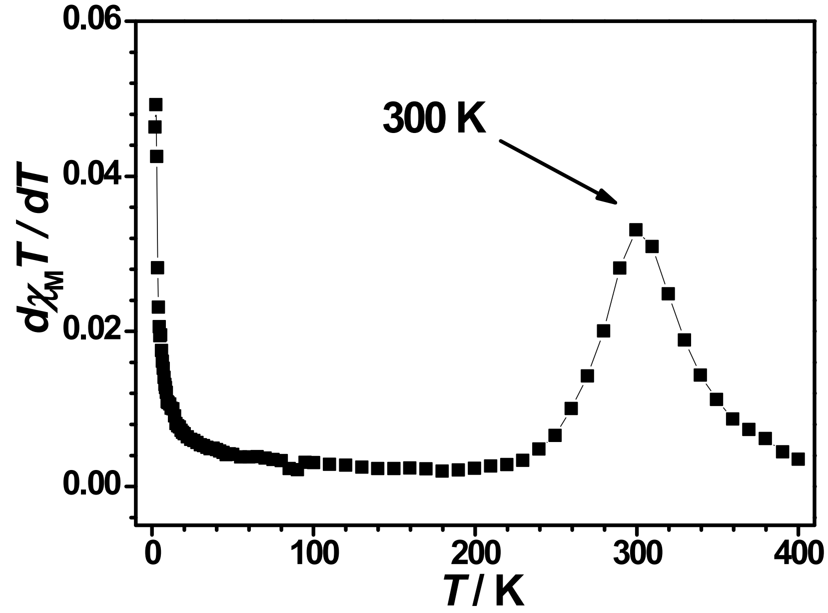

Figure S30. Plot of $d\chi_M T/dT$ *vs.* T for **2(PF$_6$)**. The $T1_{/2}$ of first step is determined as 300 K.

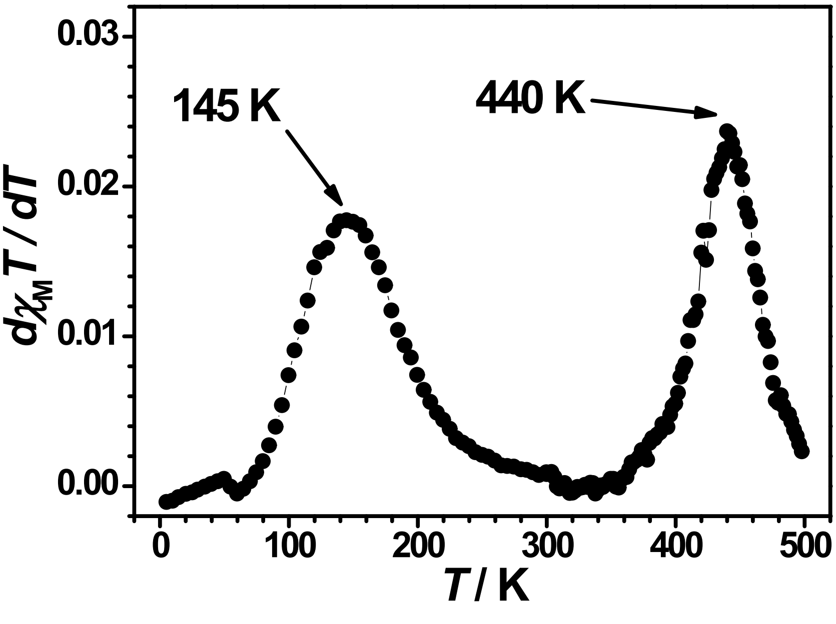

Figure S31. Plot of $d\chi_M T/dT$ *vs.* T for **2(BPh$_4$)**. The isolated two peaks at 145 and 440 K reflect the well-defined two-step SCO transition process.

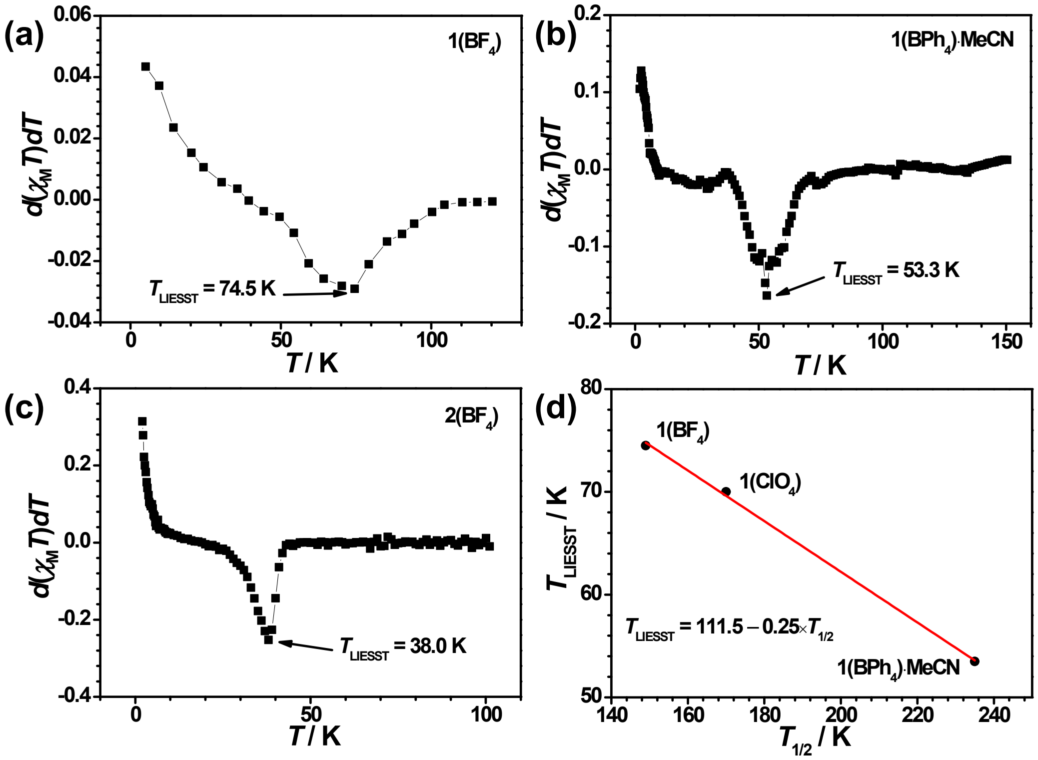

Figure S32. The T_{LIESST} temperature determined from the derivative $d(\chi_{\mathrm{M}}\mathrm{T})/dT$ plots for compounds (a) **1(BF$_4$)**, (b) **1(BPh$_4$)·MeCN**, and (c) **2(BF$_4$)**; (d) The linear fitting of T_{LIESST} *vs.* $T_{1/2}$ for **L^1** series compounds **1(ClO$_4$)**, **1(BF$_4$)**, and **1(BPh$_4$)·MeCN** (**1(ClO$_4$)**: $T_{\mathrm{LIESST}} = 70$ K, $T_{1/2} = 170$ K).

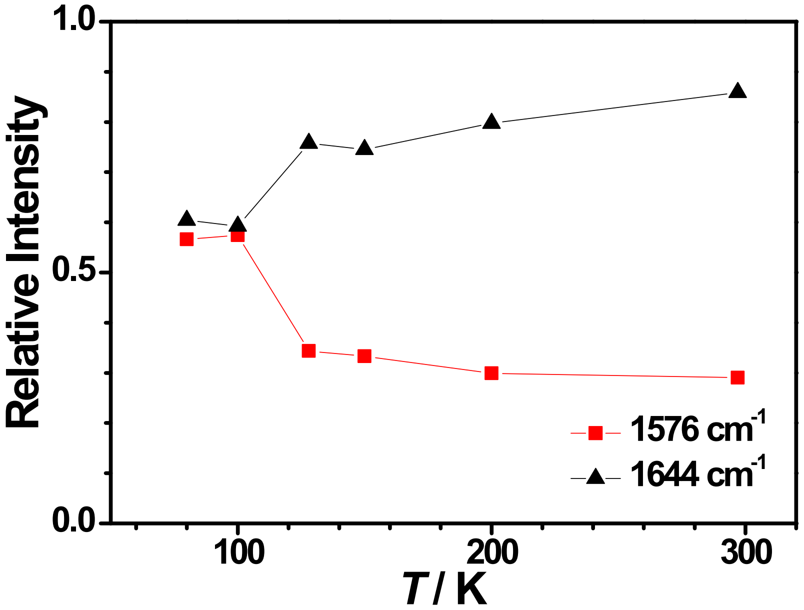

Figure S33. The change of relative intensity of peaks at 1576 cm^{-1} and 1644 cm^{-1}. The intensity of peak at 1458 cm^{-1} is defined as unit.